Bone Reports 21 (2024) 101771

Contents lists available at ScienceDirect

Bone Reports

journal homepage: www.elsevier.com/locate/bonr

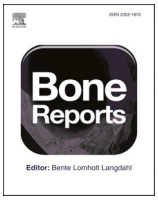

Amyloid-β neuropathology induces bone loss in male mice by suppressing bone formation and enhancing bone resorption

Younghun Jung [a,b,c,1], Birol Ay [a,1], Sajin M. Cyr [a], Christina M. Tognoni [b,c], Kaitlin Klovdahl [a], Julia Matthias [a], Qiuxia Cui [a], Daniel J. Brooks [a,e], Mary L. Bouxsein [a,e], Isabel Carreras [b,c,d], Alpaslan Dedeoglu [b,c,f], Murat Bastepe [a,*]

[a] The Endocrine Unit, Department of Medicine, Massachusetts General Hospital and Harvard Medical School, Boston, MA 02114, USA
[b] Department of Veterans Affairs, VA Boston Healthcare System, Boston, MA 02130, USA
[c] Department of Neurology, Boston University School of Medicine, Boston, MA 02118, USA
[d] Department of Biochemistry, Boston University School of Medicine, Boston, MA 02118, USA
[e] Department of Orthopedic Surgery, Beth Israel Deaconess Medical Center and Harvard Medical School, Boston, MA 02215, USA
[f] Department of Radiology, Massachusetts General Hospital and Harvard Medical School, MA 02114, USA

ARTICLE INFO

Keywords:
Alzheimer's disease
Bone metabolism
Osteoporosis
5xFAD mouse model

ABSTRACT

Alzheimer's disease (AD) and osteoporosis often coexist in the elderly. Although observational studies suggest an association between these two diseases, the pathophysiologic link between AD and skeletal health has been poorly defined. We examined the skeletal phenotype of 5xFAD mice, an AD model with accelerated neuron-specific amyloid-β accumulation causing full-blown AD phenotype by the age of 8 months. Micro-computed tomography indicated significantly lower trabecular and cortical bone parameters in 8-month-old male, but not female, 5xFAD mice than sex-matched wild-type littermates. Dynamic histomorphometry revealed reduced bone formation and increased bone resorption, and quantitative RT-PCR showed elevated skeletal RANKL gene expression in 5xFAD males. These mice also had diminished body fat percentage with unaltered lean mass, as determined by dual-energy X-ray absorptiometry (DXA), and elevated *Ucp1* mRNA levels in brown adipose tissue, consistent with increased sympathetic tone, which may contribute to the osteopenia observed in 5xFAD males. Nevertheless, no significant changes could be detected between male 5xFAD and wild-type littermates regarding the serum and skeletal concentrations of norepinephrine. Thus, brain-specific amyloid-β pathology is associated with osteopenia and appears to affect both bone formation and bone resorption. Our findings shed new light on the pathophysiologic link between Alzheimer's disease and osteoporosis.

1. Introduction

Alzheimer's disease (AD), the most common form of dementia, is an age-associated neurodegenerative disorder characterized by a progressive cognitive decline that interferes with daily life and is ultimately fatal (Blennow et al., 2006). In the United States (US), 4.5 million people are diagnosed with AD; this number is estimated to increase significantly as the population ages, and the lifespan increases (Alzheimer's Association, 2014). The pathological hallmarks of AD include the formation of extracellular amyloid-β (Aβ) plaques and intraneuronal neurofibrillary tangles of hyperphosphorylated tau protein, followed by loss of synapses and neuronal degeneration (Blennow et al., 2006). There are no known disease-reversing treatments or cures for AD, although the US Food and Drug Administration (FDA) has recently approved Aducanumab (Esang and Gupta, 2021) and Lecanemab (Larkin, 2023), which are monoclonal antibody medications that target Aβ pathology.

Another disorder prevalent in the aging population is osteoporosis, a metabolic disease characterized by reduced bone strength and increased risk of fracture, most commonly due to decreased bone mass (osteopenia) and compromised bone microarchitecture. Osteoporosis affects >10 million Americans and causes over two million fractures yearly (Benjamin, 2010; Khandelwal and Lane, 2023). Additionally, millions of

* Corresponding author at: Endocrine Unit, Department of Medicine, Massachusetts General Hospital and Harvard Medical School, 55 Fruit St, Boston, MA 02114, USA.
E-mail address: mbastepe@mgh.harvard.edu (M. Bastepe).
[1] These authors contributed equally.

https://doi.org/10.1016/j.bonr.2024.101771
Received 29 February 2024; Received in revised form 25 April 2024; Accepted 26 April 2024
Available online 28 April 2024

Americans have osteopenia and are at risk of osteoporosis (Harvey et al., 2010). Moreover, the prevalence of osteoporotic fractures is increasing by 1–3 % each year worldwide (Cummings and Melton, 2002). Osteoporosis has severe clinical consequences in the elderly, including increased mortality and, for those who survive, chronic pain and loss of independence (Black and Rosen, 2016; Compston et al., 2019). AD and osteoporosis are often comorbid in the elderly population (Peng et al., 2016; Tysiewicz-Dudek et al., 2008). Observational studies support the association between these two diseases in which i) lower bone mineral density (BMD), characteristic of osteoporosis, is associated with a higher risk of developing AD, and ii) patients with AD have reduced BMD and increased incidence of falls and hip fractures compared to age-matched controls without dementia (Bliuc et al., 2021; Chen and Lo, 2017; Kostev et al., 2018; Lv et al., 2018; Tysiewicz-Dudek et al., 2008). Whether AD and altered bone metabolism are associated as part of a common mechanism or whether there is an actual interaction between the two remains unclear.

Bone mass is regulated by the balance between bone formation and resorption, which are locally mediated by osteoblasts and osteoclasts, respectively. Multiple systemic factors regulate adult bone mass and BMD, including the availability of calcium and phosphate, the levels of certain hormones, such as vitamin D and parathyroid hormone (PTH), physical activity, and several genetic determinants. A series of locally acting paracrine signals, such as proteins of the Wnts family, allow osteoblast and osteoclast lineages to coordinate their actions. Alterations in these systemic and paracrine factors can tip the balance between bone formation and resorption via impairing osteoblast and/or osteoclast actions. The central nervous system, particularly the hypothalamus, contributes to the regulation of bone turnover through the actions of neuroendocrine hormones (Idelevich and Baron, 2018). Together with regulators of energy metabolism in the hypothalamus, the sympathetic nervous system (SNS) also plays a critical role in skeletal physiology (Elefteriou et al., 2005; Takeda et al., 2002). Mediating SNS activity, the adrenergic signaling inhibits osteoblast proliferation and function and increases the level of the major osteoclastogenic cytokine receptor activator of nuclear factor kappa-B ligand (RANKL), thereby promoting bone resorption (Elefteriou et al., 2005; Takeda et al., 2002). The SNS is also involved in synchronizing peripheral tissues with the master “clock” in the hypothalamic suprachiasmatic nucleus (Okamura, 2007), and certain skeletal effects of SNS are associated with altered expression levels of genes regulating the circadian rhythm (Fu et al., 2005). Studies have shown that ablating clock genes in mice, such as *Bmal1*, encoding the core circadian regulator aryl hydrocarbon receptor nuclear translocator-like protein 1 (BMAL1, also known as ARNTL), results in abnormal bone remodeling (Fu et al., 2005; Qian et al., 2020; Samsa et al., 2016; Takarada et al., 2017).

Hypothalamic dysfunction has been established in AD patients (Ishii and Iadecola, 2015; Vercruysse et al., 2018), and the reduced BMD found in AD has been positively associated with reduced grey matter volume of the hypothalamus (Loskutova et al., 2010; Saper and German, 1987). As an indication of hypothalamic dysfunction, AD patients display increased SNS activity with elevated norepinephrine levels (Elrod et al., 1997; Pascualy et al., 2000; Raskind et al., 1988; Szot et al., 2000). Moreover, a perturbed circadian rhythm has been observed frequently in AD patients, worsening with disease progression (Musiek et al., 2015, 2018). In fact, aberrant expression of *BMAL1* has been found in AD brain samples and cultured AD patient-derived fibroblasts, indicating systemic circadian clock alterations (Cronin et al., 2017). Nonetheless, whether AD-associated osteoporosis results from abnormalities related to Aβ-induced hypothalamic dysfunction has remained unclear.

Previous mouse studies have explored the relationship between Aβ pathology and osteoporosis. Low BMD and osteopenia were detected in Tg2576 mice (also known as APPswe), which express a human Swedish familial mutation of the gene encoding amyloid precursor protein (APP) under the control of the hamster prion promoter (Cui et al., 2011; Xia et al., 2013), and in APP/PS1 mice, which express a chimeric mouse/human APP and a mutant human presenilin 1 (PSEN1) driven by the mouse prion promoter (Peng et al., 2014; Yang et al., 2011). However, the transgene in each of these AD mouse models was found to be expressed not only in the brain but also in bone, indicating that the bone phenotype resulted, at least partly, from cell-autonomous actions of the disease-causing APP or PSEN1 mutants in the osteoclast and osteoblast lineages (Cui et al., 2011; Xia et al., 2013). Hence, whether the Aβ neuropathology can influence bone metabolism has remained uncertain.

Here, we investigated the skeletal phenotype of 5xFAD mice, a mouse model of accelerated Aβ neuropathology, in which the expression of five familial AD mutations in human amyloid precursor protein (APP) and presenilin 1 (PSEN1) genes are driven by a murine Thy1 promoter modified to exclude extra-neuronal control elements (Moechars et al., 1996; Oakley et al., 2006; Vidal et al., 1990). After verifying the absence of transgene expression in bone, bone marrow, and bone marrow stromal cells (BMSCs), we revealed osteopenia in 8-month-old male, but not female, 5xFAD mice. Additional analyses of male 5xFAD mice indicated a reduced bone formation rate, increased bone resorption parameters, and increased skeletal RANKL expression levels. Male 5xFAD mice also showed systemic signs of elevated SNS activity, with reduced fat percentage and increased *Ucp1* expression in brown fat.

2. Materials and methods

2.1. Mice

Male and female five familial Alzheimer's disease (5xFAD) transgenic mice and non-transgenic wildtype (WT) littermates as controls were used in this study. Maintained in the B6SJL background, 5xFAD mice co-express the human APP and PSEN1 genes harboring a total of 5 familial AD mutations [APP K670N/M671L (Swedish) + I716V (Florida) + V717I (London) and PS1 M146L + L286V] under the control of the murine Thy1 promoter devoid of the extra-neuronal control elements (#034840-JAX) (Moechars et al., 1996; Oakley et al., 2006; Vidal et al., 1990). Mice were housed on a 12 h light:12 h dark schedule. All mice were given access to food and water ad libitum. 5xFAD and WT littermates were randomized for inclusion in the analysis groups. Body weight measurements and μCT analyses were conducted in male and female 8-month-old 5xFAD and WT littermates. Since bone loss was observed in male, but not female 5xFAD mice, the rest of the experiments employed male mice only. The experimental design with outcome measures, sample size, sex, age, and individual batches of mice analyzed are outlined in Supplementary Table S1.

2.2. Ethics approval

All animal experiments were carried out in accordance with the National Institute of Health (NIH) Guide for the Care and Use of Laboratory Animals and were approved by the research animal care committee at VA Boston Healthcare System and Massachusetts General Hospital and Harvard Medical School. All methods comply with the ARRIVE guidelines (Percie du Sert et al., 2020).

2.3. Tissue collection and bone marrow stromal cell isolation

Mice were euthanized by CO_2 asphyxiation. The cerebral cortex of the right hemisphere of brain tissues, hypothalamus, brown adipose tissues (BAT), and kidney were dissected and stored at —80C until RNA extraction. Femurs were cleaned from surrounding muscle tissue. Proximal and distal ends of one femur were cut with scissors, and bone marrow was separated from the femur by centrifugation at 6000 ×*g* for 30 s. Femur and bone marrow were then snap-frozen in liquid nitrogen and stored at —80C until RNA extraction. The femur was fixed with 80 % ethanol for μCT or histomorphometry. For isolating BMSCs, both femurs were extracted from 8-month-old male mice, cleaned from surrounding soft tissue, and washed twice with PBS containing 1 %

antibiotics (catalog no. 30-004-CI, Corning). Proximal and distal ends of the femurs were cut with scissors, and marrow cells were flushed out by a needle and syringe containing complete medium (alpha-MEM containing 10 % fetal bovine serum, and 1 % antibiotics). Thereafter, the cells were cultured at a density of 0.5×10^6 to 1×10^6 cells/cm^2 in the complete medium for seven days. Adherent cells were collected, as described (Cui et al., 2021).

2.4. Imaging analyses

MicroCT analysis was performed on the distal femurs from WT and 5xFAD mice, using a high-resolution desktop micro-tomographic imaging system (μCT40, Scanco Medical AG, Brüttisellen, Switzerland). Scans were acquired using a 10 μm^3 isotropic voxel size, 70 kVP, 114 μA, 200 ms integration time, and were subjected to Gaussian filtration and segmentation. Image acquisition and analysis protocols adhered to the guidelines for assessing rodent bones using μCT (Bouxsein et al., 2010). Dual-energy X-ray absorptiometry (DXA) scans (Lunar PIXImus2, General Electric) were performed to determine the whole body (except for the head) bone mineral density, body fat percentage, and lean mass according to the manufacturer's directions. Areal BMD was transformed to volumetric BMD (vBMD, also known as bone mineral apparent density) by dividing by the square root of the bone area, as previously described (Carter et al., 1992). Imaging analyses were conducted at the MGH Center for Skeletal Research Imaging and Biomechanical Testing Core.

2.5. Dynamic histomorphometry

To label the newly formed bone, two doses of calcein (25 mg/kg, catalog no. C0875, Sigma-Aldrich) were injected intraperitoneally (*i.p.*) to 8-month-old male WT and 5xFAD mice eight days apart. Seventy-two hours after the second calcein injection, mice were euthanized for tissue harvest. Tissue processing and histomorphometry on the distal portion of the femur were performed at the MGH Center for Skeletal Research Histology & Histomorphometry Core according to the American Society for Bone and Mineral Research guidelines (Dempster et al., 2013). The Masson's Trichrome stain kit from Thermo Fisher (catalog no. 87019) was used to visualize osteoblasts, and the Leukocyte Acid Phosphatase (TRAP) Kit from Sigma-Aldrich (catalog no. 387A) was used to identify osteoclasts, with Fast Green (catalog no. F7252, Sigma-Aldrich) as counterstaining.

2.6. Calcium, phosphate, FGF23, norepinephrine, and Aβ42 measurements

Mice were anesthetized with 1–3 % *isoflurane*. Blood was collected from the retroorbital vein into heparin blood collection tubes to prepare plasma. Plasma norepinephrine levels were measured using the Noradrenaline (Norepinephrine) High Sensitive ELISA kit (catalog no. NOU39-K01, Eagle Biosciences). Bone norepinephrine levels were measured using the same kit, essentially as previously described (Zhu et al., 2018). Briefly, femurs devoid of marrow and epiphyses were snap-frozen, pulverized, and resuspended in an acidic extraction buffer containing 0.01 N HCL, 0.15 mM EDTA, and 4 mM sodium metabisulfite. The lysates were neutralized with a 10 % volume of 1.0 M Tris pH 8.0 and subsequently analyzed by ELISA. Norepinephrine levels were normalized to the amount of protein in the bone sample, measured by the BCA protein assay kit (catalog no. 23227, Thermo Fisher). Serum total calcium and phosphate were quantified using a kit from Stanbio (Procedure No. 0150) or Abcam (catalog no. ab65622), respectively. Serum intact FGF23 levels were measured by an ELISA kit (catalog no. 60-6800, Quidel). Hypothalamus tissue was homogenized with 5 volumes (*w/v*) of Tris-buffered saline (TBS). The soluble protein fraction was obtained by centrifugation at 100,000*g* for 1 h at 4 °C and used to quantify the concentration of soluble Aβ42 using an ELISA kit (catalog no. KMB3441, Invitrogen).

2.7. Reverse-transcription polymerase chain reaction

Total RNA was extracted from different tissues and BMSCs from 8-month-old male WT and 5xFAD mice using the RNeasy Mini Kit (catalog no. 74104, Qiagen) and converted into cDNA using a First-Strand Synthesis Kit (catalog no. E6560, New England BioLabs) with or without reverse transcriptase. Bone tissue consisted of cortical bone devoid of marrow. Frozen bone samples were pulverized before resuspension in TRIzol Reagent (catalog no. 15596018, Invitrogen) and subsequently subjected to column purification using the RNeasy Mini Kit. Regular reverse-transcription PCR was performed to detect the transgene-derived expression of the human presenilin (PSEN1) transcript. For quantitative RT-PCR (qRT-PCR) analysis, an Applied Biosystems QuantStudio 3D Digital PCR System (Applied Biosystems) was employed with PowerUp SYBR Green qPCR Master Mix (catalog no. A25742, Applied Biosystems) according to the directions of the manufacturer. The amplification linearity and specificity of amplicons were tested by using different amounts of cDNA template and by verifying melting temperature curves, respectively. *Fgf23* gene expression was detected with TaqMan MGB probes (*Fgf23*, Mm00437132_m1; *β-actin*, Mm00607939_s1) using TaqMan™ Fast Advanced Master Mix (4444557, Applied Biosystems). Primer sequences are provided in Supplementary Table S2.

2.8. Statistical analyses

Our power analysis determined a minimum sample size of 5, using Z-statistics with an alpha (Type-I error) of 0.05 (two-tailed), a beta (Type-II error) of 0.2 (i.e., 80 % power), and a standard effect size of 1.8 (based on initial BV/TV values) or 2.2 (based on initial BMD values). The standard effect size is calculated by dividing the difference between the means by the standard deviation. Results are presented as individual data points alongside means. Single outliers in individual data sets, if any, were identified by the Grubbs test and excluded before analyses. After confirming that the data sets were normally distributed (using Shapiro-Wilk and Kolmogorov-Smirnov tests), an unpaired two-tailed Student's t-test was utilized to test the significance of the difference between two groups. Welch's correction was applied if the variances were significantly different, as determined by the F test. Two-way ANOVA with Tukey's posthoc test was performed to assess the statistical significance of differences between skeletal findings of male WT and 5xFAD mice at ages 5 and 8 months. Values of $P < 0.05$ were considered significant. Statistical analyses were performed using GraphPad Prism version 10.1.1.

3. Results

3.1. The mutant transgene expression is not detectable in 5xFAD mouse bones

To study the influence of Aβ neuropathology on bone remodeling, we chose the 5xFAD mouse model because the transgene-derived mutant APP and PSEN1 proteins are both expressed by the mouse Thy1 promoter modified to lack extra-neuronal elements (Moechars et al., 1996; Oakley et al., 2006; Vidal et al., 1990). As expected, our RT-PCR assays showed that the transgene-derived human *PSEN1* mRNA was expressed in the brain tissue but not in whole bones (without the marrow), the bone marrow, or BMSCs from 8-month-old male 5xFAD mice (Fig. 1A). RT-PCR reactions without reverse transcriptase, used as negative controls, did not show any amplification, nor did any of the tissues from WT controls (Fig. 1A). These findings strongly suggested that the mutant transgenes are not expressed in bone cells, hematopoietic cells, or skeletal stem/progenitor cells of 5xFAD mice.

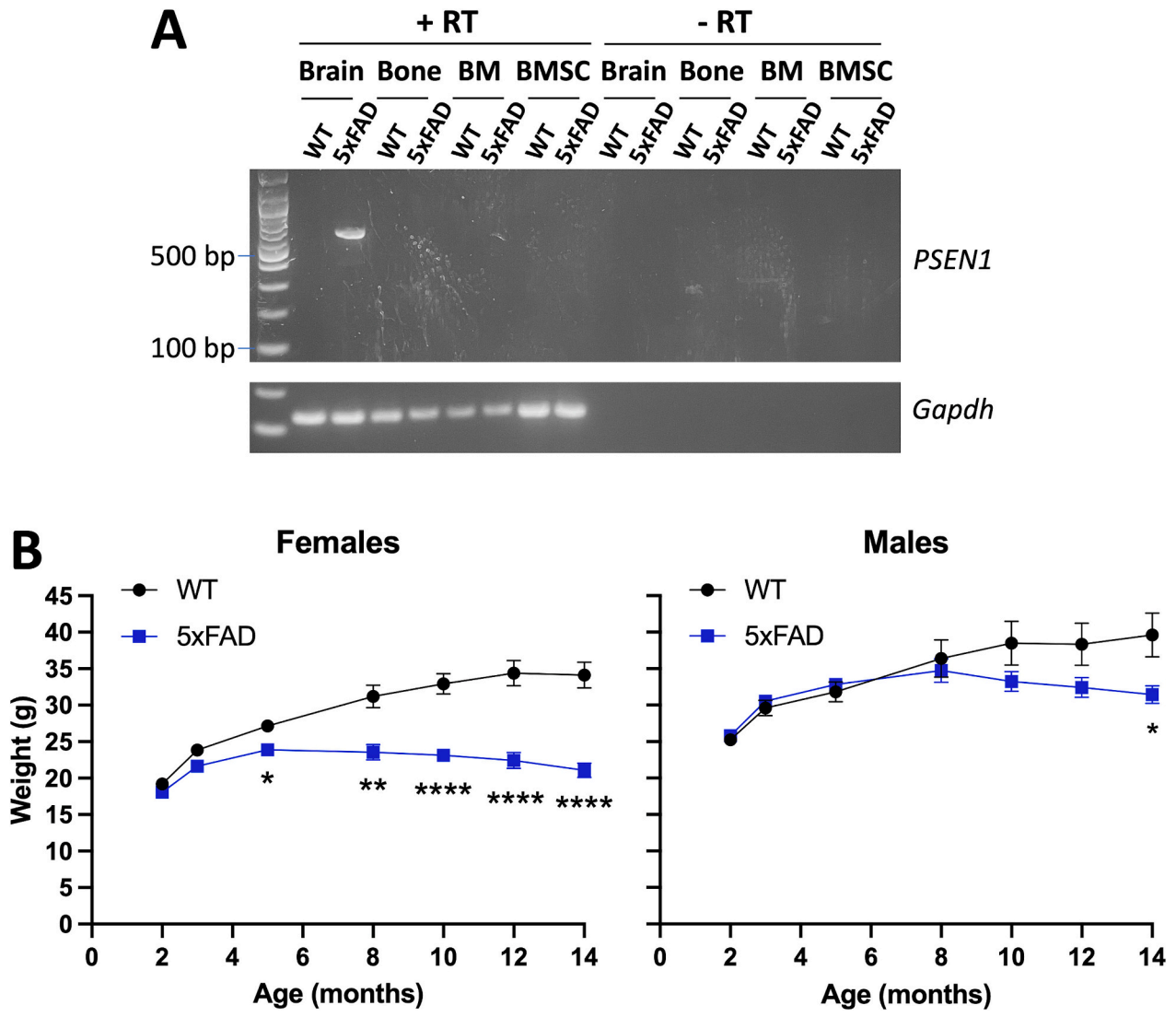

Fig. 1. AD transgene expression in the bone, bone marrow, and BMSCs and the body weights of 5xFAD and WT littermates. (A) RT-PCR with reaction conditions including (+RT) or excluding (−RT) reverse transcriptase was used to amplify human *PSEN1* mRNA in the whole brain, bone (marrow flushed-out), bone marrow (BM), and bone marrow stromal cells (BMSCs) from male WT and 5xFAD mice at 8 months of age. The first lane was loaded with a 100-bp DNA ladder. Gel images were acquired with ChemiDoc MP imaging system (BioRad). (B) Body weight measurements of female and male 5xFAD and WT littermates over time. Data are mean ± SEM (n = 9–12 mice per group). *, $P < 0.05$; **, $p < 0.01$; ****, $p < 0.0001$ vs. age-matched WT by Student's t-test.

3.2. Male but not female 5xFAD mice exhibit reduced bone mass

In the brain of 5xFAD mice, intraneuronal Aβ42 is detectable in the cortex and the subiculum region of the hippocampus starting around 1.5 months of age, with significant extracellular amyloid deposition in these regions by three months of age (Oakley et al., 2006). By age 6–8 months, amyloid plaques spread throughout the hippocampus and cortex, with gliosis, synapse degeneration, neuron loss, and cognitive deficits (Oakley et al., 2006). Mechanical loading maintains bone mass; therefore, reduced body weight may be associated with low bone mass (Iwaniec and Turner, 2016). While significant weight loss was evident in female 5xFAD mice starting from age 5 months, the body weights of males remained comparable in WT and 5xFAD mice at least until eight months of age (Fig. 1B). To assess the skeletal phenotype associated with severe AD neuropathology, we performed μCT of femurs from 8-month-old WT and 5xFAD mice. Despite having significantly reduced body weights, female 5xFAD mice did not differ from female WT littermates in any of the parameters measured (Table 1). In contrast, male 5xFAD mice displayed diminished bone volume-to-total volume ratio (BV/TV; ~36 % of WT) and BMD (~49 % of WT), differing significantly from male WT littermates in multiple trabecular and cortical bone parameters (Table 1 and Fig. 2A, B). Because male 5xFAD mice, unlike female 5xFAD mice, lacked significantly diminished body weight yet exhibited osteopenia, we performed our further studies using male mice. To determine if the bone loss manifests at a younger age, we examined the skeletal phenotypes of 5-month-old males and detected modest reductions in the trabecular number and connectivity density with increased trabecular separation in femurs from 5xFAD compared to WT littermates; no significant differences were observed in the other parameters analyzed (Table 2). Indeed, the 5-month-old male mice (both WT and 5xFAD) showed significantly higher BV/TV, BMD, and trabecular thickness compared to 8-month-old 5xFAD males (Fig. 2C-E, Supplementary Table S3). Moreover, the significant increase of cortical area, cortical bone mineral density, and cortical thickness observed in WT male mice from age 5 to 8 months was not detected in 5xFAD male littermates (Fig. 2F-H, Supplementary Table S3). These results indicate that 5xFAD males develop substantial osteopenia between ages 5 and 8 months, i.e., when the brain Aβ neuropathology progresses from moderate to severe.

Table 1
Micro-computed tomography analysis of femoral bone from 8-month-old WT and 5xFAD littermates.

	Female			Male		
	WT (n = 5)	5xFAD (n = 5)	P*	WT (n = 5)	5xFAD (n = 5)	P*
Distal femoral metaphysis						
BV/TV (%)	9.56 ± 2.71	10.62 ± 2.56	0.784	19.80 ± 3.14	7.04 ± 1.32	0.006
ConnD. (1/mm^3)	39.4 ± 11.2	51.9 ± 21.8	0.622	83.3 ± 12.6	46.1 ± 11.3	0.059
BMD (mgHA/cm^3)	165.4 ± 31.3	184.5 ± 31.0	0.676	274.7 ± 33.1	135.5 ± 15.3	0.005
SMI	2.18 ± 0.39	2.02 ± 0.27	0.734	1.09 ± 0.31	2.43 ± 0.18	0.006
Tb.N (1/mm)	2.73 ± 0.37	2.90 ± 0.43	0.766	3.51 ± 0.36	3.31 ± 0.17	0.620
Tb.Th (mm)	0.059 ± 0.004	0.061 ± 0.005	0.747	0.067 ± 0.002	0.042 ± 0.002	0.00002
Tb.Sp (mm)	0.403 ± 0.075	0.386 ± 0.082	0.877	0.291 ± 0.030	0.300 ± 0.016	0.795
Femoral midshaft						
Tt.Ar [mm^2]	1.73 ± 0.06	1.75 ± 0.04	0.723	2.16 ± 0.04	2.08 ± 0.11	0.474
Ct.Ar [mm^2]	0.929 ± 0.031	0.956 ± 0.053	0.673	1.228 ± 0.039	0.941 ± 0.037	0.001
Ct. Th (mm)	0.227 ± 0.006	0.233 ± 0.013	0.712	0.266 ± 0.012	0.196 ± 0.005	0.001
Ct. TMD (mgHA/cm^3)	1321 ± 6	1335 ± 9	0.255	1325 ± 5	1270 ± 11	0.002
Ct.Ar/Tt.Ar (%)	53.9 ± 1.3	54.5 ± 2.1	0.823	56.8 ± 2.2	45.4 ± 1.7	0.003
Ct. Porosity (%)	0.462 ± 0.021	0.476 ± 0.023	0.665	0.660 ± 0.062	0.676 ± 0.085	0.883
pMOI[mm^4]	0.391 ± 0.024	0.403 ± 0.025	0.742	0.656 ± 0.025	0.519 ± 0.046	0.031
Imax[mm^4]	0.255 ± 0.017	0.258 ± 0.017	0.891	0.450 ± 0.025	0.355 ± 0.030	0.042
Imin[mm^4]	0.136 ± 0.008	0.145 ± 0.010	0.510	0.206 ± 0.007	0.164 ± 0.016	0.047

Data represent mean ± S.E.M, *Student's t-test, n = 5 mice per group.
Bone volume per trabecular volume (BV/TV), connectivity (ConnD), bone mineral density (BMD), structure model index (SMI), trabecular number (Tb. N), trabecular thickness (Tb. Th), trabecular separation (Tb. Sp), total area (Tt. Ar), cortical area (Ct. Ar), cortical thickness (Cor. Th), cortical tissue mineral density (Ct. TMD), cortical area per total area (Ct.Ar/Tt.Ar), cortical porosity (Ct. Porosity), polar moment of inertia (pMOI), maximum moment of inertia (Imax), minimum moment of inertia (Imin).

3.3. 5xFAD males have decreased bone formation and increased bone resorption

Insufficient circulating levels of calcium or phosphate can impair bone mineralization and reduce BMD. However, we did not detect altered serum calcium or phosphate levels in 8-month-old male 5xFAD mice (Supplementary Fig. S1). To understand the cellular mechanism of osteopenia, we then performed dynamic histomorphometry of distal femurs from 8-month-old male 5xFAD and WT littermates. Consistent with the μCT data collected, we detected a significant reduction of bone volume in 5xFAD males (BV/TV = 9.12 ± 0.84 vs. 14.11 ± 1.36 % in WT, $P = 0.004$). Bones from 5xFAD males also showed lower osteoblast surface per bone perimeter and numbers of osteoblasts per bone surface with normal numbers of osteocytes per trabecular bone area (Fig. 3A and Fig. 4A-C). Moreover, bone formation parameters, including mineral apposition and bone formation rates, were significantly reduced (~64 % and 41 % of WT, respectively) (Fig. 3B and Fig. 4D-F). In contrast, several bone resorption markers were elevated in 5xFAD mice compared to WT littermates, such as osteoclast surface (~137 % of WT) and erosion surface per bone surface (~134 % of WT) and osteoclast number for bone perimeter (~156 % of WT) (Fig. 3C and Fig. 4G-I). Together, these findings indicated reduced bone formation and increased bone resorption in 5xFAD males.

The Wnt/β-catenin signaling pathway positively regulates bone formation by stimulating the proliferation and differentiation of osteoprogenitors (Baron and Gori, 2018; Craig et al., 2023; Karner and Long, 2017). We found diminished skeletal expression levels of Wnt/β-catenin signaling targets *Axin2* and *Tcf7* in male 5xFAD mice compared to WT littermates, although statistical significance was not reached (Fig. 5A). Among the gene targets of Wnt signaling in osteocytes are *Dkk1* and *Sost*, which encode secreted Wnt antagonists Dickkopf Wnt Signaling Pathway Inhibitor 1 and sclerostin, respectively. We found that the skeletal expression level of *Dkk1* was not altered, whereas the level of *Sost* appeared lower in male 5xFAD than WT mice (albeit statistically not significant; $P = 0.16$) (Fig. 5A). Also displaying a trend toward diminished expression levels was another osteocyte-specific gene *Ffg23*, whose expression is positively associated with Wnt signaling (Lavi-Moshayoff et al., 2010; Liu et al., 2009; Nagata et al., 2022). *Fgf23* encodes the phosphaturic hormone fibroblast growth factor-23 (FGF23) (Fig. 5A). Indeed, the circulating levels of FGF23 in 8-month-old 5xFAD males were significantly lower than in WT male littermates (Supplementary Fig. S2). These results collectively indicated that 5xFAD males may have reduced skeletal Wnt/β-catenin signaling. Since the balance between RANKL and osteoprotegerin (OPG) plays a crucial role in osteoclastogenesis, we also measured mRNA levels of *Tnfsf11* (encoding RANKL) and *Tnfrsf11b* (encoding OPG). The RANKL expression level in femurs from 5xFAD males was significantly higher than WT controls (~176 % of WT), while OPG levels were comparable (Fig. 5B), with a trend toward elevated RANKL/OPG ratio (Fig. 5C). These findings suggest that the enhanced bone resorption parameters are due, at least partly, to increased osteoclastogenesis.

3.4. Hypothalamic involvement of AD neuropathology in 5xFAD mice

Since hypothalamic dysfunction could result in dysregulated bone turnover, we first verified that Aβ accumulation was present in the hypothalamus of 8-month-old 5xFAD males. ELISA assays for soluble Aβ42 protein measured 258 ± 65 pg/mg tissue for 5xFAD vs. below detection level for WT in hypothalamus lysates ($n = 10$ per genotype). Besides bone remodeling, the hypothalamus regulates body composition. DXA scans showed that, in addition to decreased vBMD (Fig. 6A), the male 5xFAD mice displayed significantly lower body fat percentage (~73 % of WT) with no change in lean mass (Fig. 6B, C). Since reduced fat percentage can be due to increased SNS activity, we measured *Ucp1* mRNA levels in brown adipose tissue (BAT), a sensitive indicator of increased SNS tone in mice (Thomas and Palmiter, 1997). We found significantly augmented levels *Ucp1* mRNA (~159 % of WT) in 8-month-old male 5xFAD mice (Fig. 6D). However, while this finding was consistent with elevated SNS tone, plasma norepinephrine levels did not differ significantly between male 5xFAD and WT littermates (Fig. 6E). The norepinephrine levels in bone were also comparable between male 5xFAD and WT mice (Fig. 6F).

Increased SNS tone mediates the effects of leptin on bone remodeling, which are associated with altered expression levels of circadian rhythm genes in the bone (Fu et al., 2005). Since circadian rhythm disturbances are also found frequently in AD patients (Musiek et al.,

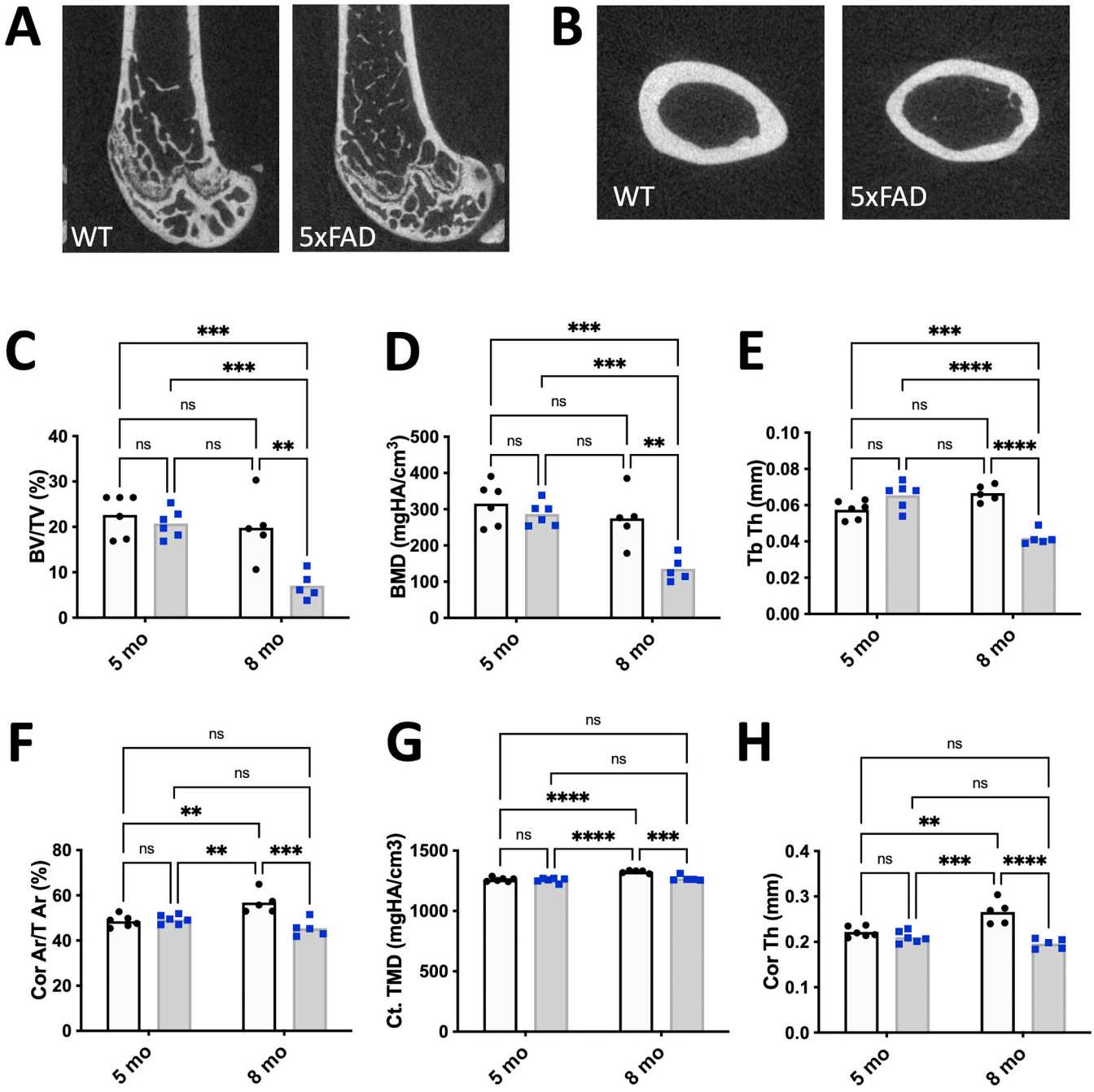

Fig. 2. Micro-computed tomography (μCT) indicates reduced bone mass in 8-month-old male 5xFAD mice. (A, B) μCT images of the distal femur and femoral midshaft, respectively, in 8-month-old male WT and 5xFAD mice. (C—H) μCT analysis of femoral trabecular and cortical bone in 5- and 8- month-old WT and 5xFAD littermates. Bone volume per trabecular volume (BV/TV), cortical bone area per total area (Cor Ar/T Ar), bone mineral density (BMD), cortical tissue mineral density (Ct. TMD), trabecular thickness (Tb. Th), and cortical thickness (Cor. Th). Data represent individual points and mean. **, $P < 0.01$; ***, $P < 0.001$; ****, $P < 0.0001$ by 2-way ANOVA with Tukey's posthoc test; ns, not significant; $n = 5$–6 mice per group. See also Tables 1 and 2.

2015, 2018), we analyzed the skeletal mRNA levels of *Bmal1* and *Clock* (encoding circadian locomotor output cycles kaput, the main heterotrimeric partner of BMAL1). We also examined the mRNA levels of genes induced by BMAL1/CLOCK, including *Per1/2* and *Cry1/2*, encoding period 1 and 2 and cryptochrome 1 and 2, respectively, which in turn inhibit BMAL/CLOCK in a negative regulatory loop (Bolsius et al., 2021). Femurs of 8-month-old male 5xFAD mice exhibited markedly diminished mRNA levels of *Bmal1* (~29 % of WT), while the levels of *Clock*, *Per1/2*, and *Cry1/2* were not significantly changed (Fig. 7A); however, *Clock* and *Per1* expression tended to be decreased or increased, respectively. In addition to CLOCK, BMAL1 heterodimerizes with neuronal PAS domain protein 2 (NPAS2) (Bolsius et al., 2021). However, we did not find any alteration in the skeletal expression level of the *Npas2* gene (Fig. 7B). To explore the underlying cause of *Bmal1* reduction in bone, we then measured the expression levels of *Rora* and *Nr1d1* (also known as *Rev-Erbα*), encoding RAR-related orphan receptor A and receptor subfamily 1, group D, member 1, respectively. These genes are also induced by BMAL1/CLOCK, but the protein product of each either activates or represses *Bmal1* transcription in a secondary regulatory loop (Bolsius et al., 2021). Male 5xFAD femurs exhibited significantly reduced mRNA levels of *Rora* (~68 % of WT) and tended to have lower levels of *Nr1d1* compared to male WT littermates (Fig. 7B), consistent

Table 2
Micro-computed tomography analysis of femoral bone from 5-month-old male WT and 5xFAD littermates.

	WT ($n = 6$)		5xFAD (n = 6)		P*
Distal femoral metaphysis					
BV/TV (%)	22.66	±1.88	20.76	±1.27	0.421
ConnD. (1/mm^3)	153.2	±9.9	101.9	±8.9	0.003
BMD (mgHA/cm^3)	315.6	±24.0	287.0	±13.5	0.323
SMI	0.89	±0.17	1.15	±0.06	0.172
Tb.N (1/mm)	4.81	±0.27	3.84	±0.20	0.017
Tb.Th (mm)	0.058	±0.002	0.066	±0.003	0.050
Tb.Sp (mm)	0.201	±0.013	0.260	±0.016	0.017
Femoral midshaft					
Tt.Ar [mm^2]	2.23	±0.11	2.02	±0.08	0.161
Ct.Ar [mm^2]	1.079	±0.040	0.995	±0.033	0.136
Ct. Th (mm)	0.222	±0.005	0.211	±0.005	0.147
Ct. TMD (mgHA/cm^3)	1261	±7	1256	±8	0.667
Ct.Ar/Tt.Ar (%)	48.5	±1.1	49.3	±0.8	0.608
Ct. Porosity (%)	0.193	±0.010	0.219	±0.018	0.250
pMOI[mm^4]	0.618	±0.055	0.516	±0.041	0.166
Imax[mm^4]	0.408	±0.037	0.347	±0.033	0.243
Imin[mm^4]	0.209	±0.021	0.169	±0.011	0.114

Data represent mean ± S.E.M, *Student's t-test, n = 6 mice per group.
Bone volume per trabecular volume (BV/TV), connectivity (ConnD), bone mineral density (BMD), structure model index (SMI), trabecular number (Tb. N), trabecular thickness (Tb. Th), trabecular separation (Tb. Sp), total area (Tt. Ar), cortical area (Ct. Ar), cortical thickness (Cor. Th), cortical tissue mineral density (Ct. TMD), cortical area per total area (Ct.Ar/Tt.Ar), cortical porosity (Ct. Porosity), polar moment of inertia (pMOI), maximum moment of inertia (Imax), minimum moment of inertia (Imin).

with the reduced *Bmal1* expression level. These findings suggested that the skeletal circadian rhythm may be perturbed in 8-month-old male 5xFAD mice. A study showed abnormal BMAL1 levels in the brain and fibroblasts of AD patients (Cronin et al., 2017). Therefore, we checked the *Bmal1* expression level in several additional tissues. While no significant differences were detected between 5xFAD and WT males in the bone marrow, BAT, or hypothalamus, we found significantly reduced *Bmal1* mRNA levels in the kidney of male 5xFAD mice (Fig. 7C), suggesting that bone may not be the only tissue in which clock genes are dysregulated.

4. Discussion

We studied the influence of Aβ-driven neuropathology on bone by analyzing the skeletal phenotype of 5xFAD mice, which develop a full-blown AD-like phenotype by the age of 8 months. We showed that male, but not female, 5xFAD mice display progressive bone loss that is significant by the age of 8 months. The Thy1 promoter used in 5xFAD mice has been modified to exclude extra-neuronal elements, unlike the endogenous Thy1 promoter, which is also active in some osteoblast lineage cells (Chen et al., 1999). As predicted, we did not detect the AD transgene expression in the femur, bone marrow, or BMSCs. After removal of the marrow, long bones are enriched for osteoblast lineage cells, including mature osteoblasts and osteocytes, but also comprise a range of different cell types, including mesenchymal, endothelial, and hematopoietic cells (Ayturk et al., 2020). The most abundant cells in the bone marrow are of hematopoietic origin, including myeloid lineage progenitor cells giving rise to osteoclasts (Xing et al., 2005). Bone marrow contains several additional cell types, including mesenchymal skeletal stem and endothelial cells (Baryawno et al., 2019). BMSCs represent multipotent skeletal stem cells (Arora and Robey, 2022; Sivaraj et al., 2021). Thus, being unable to detect transgene expression in 5xFAD mice by RT-PCR in these tissues and cells strongly suggests that the observed skeletal phenotype of male 5xFAD mice reflects an influence of brain pathology on bone turnover rather than a local effect of the mutant transgenes.

Interestingly, female WT and 5xFAD mice displayed no differences in skeletal phenotypes at age 8 months, even though these mice exhibited significant weight loss at this age and are known to have more severe AD-like neuropathology than their male counterparts (Marazuela et al., 2022). Thus, it is likely that other factors than those derived from the neuronal accumulation of Aβ are involved in the skeletal phenotype, either protecting the females from AD-induced bone loss or making the males much more susceptible to this effect than females. Further investigations of this model may explain the observed sexual dimorphism in the bone phenotype and reveal new sex-specific mechanisms governing bone turnover in AD. However, previous studies have shown that age-related bone loss is substantially more prominent in female than in male C57BL/6 J mice, with differences detected by μCT becoming evident as early as two months of age (Glatt et al., 2007). Thus, rather than a true sex-specific difference in how AD-like brain pathology influences bone remodeling, the absence of osteopenia in female 5xFAD mice may reflect the masking of AD-related skeletal phenotype by age-related bone loss.

Our dynamic histomorphometry analyses show that 8-month-old male 5xFAD mice have increased osteoclast and decreased osteoblast numbers/function, with a significantly decreased bone formation rate. Although our whole femur gene expression analyses have limitations due to the multiplicity of cell types included, the results provide suggestions regarding the underlying mechanisms. The increased osteoclast numbers/function may be the outcome, at least partly, of increased skeletal RANKL levels since this cytokine, secreted by osteoblasts and osteocytes, promotes the differentiation of osteoclasts from bone marrow macrophages.

The trend toward low skeletal expression levels of *Axin2* and *Tcf7* we detected in 8-month-old male 5xFAD mice may indicate suppressed Wnt/β-catenin signaling. Further support for this conclusion is the significantly diminished serum FGF23 concentrations with a trend toward reduced skeletal *Fgf23* gene expression, given that some studies showed blunted FGF23 synthesis upon blocking Wnt signaling (Lavi-Moshayoff et al., 2010; Nagata et al., 2022), and a mouse model of excess FGF23 production has an amplified Wnt signaling pathway in bone (Liu et al., 2009). If true, the decrease in Wnt/β-catenin signaling may explain, at least partly, the impaired bone formation. A previous study has revealed a reduction in the Wnt/β-catenin pathway in the bone and brain of a mouse model of tau pathology, which also shows decreased BMD (Dengler-Crish et al., 2018, 2016). Hence, different underlying AD neuropathologies may converge on the Wnt/β-catenin signaling pathway in influencing bone remodeling. The tendency for reduced skeletal expression levels of osteocyte-specific gene *Sost* (Yoshioka et al., 2021; Youlten et al., 2021) may be due to an overall reduction of osteocyte numbers, considering that the osteocyte density was unaltered despite reduced BV/TV in 5xFAD mice; however, a defect in osteocyte function cannot be ruled out.

The central nervous system, particularly the hypothalamus, contributes to the regulation of bone turnover (Canet et al., 2018; Dimitri and Rosen, 2017; Driessler and Baldock, 2010; Idelevich and Baron, 2018), and hypothalamic dysfunction has been established in AD patients (Ishii and Iadecola, 2015; Vercruysse et al., 2018). The reduced body fat percentage with a normal lean mass and the significantly increased brown fat levels of *Ucp1* expression suggest elevated SNS activity in 8-month-old male 5xFAD mice. Increased SNS activation causes impaired bone formation and enhanced bone resorption associated with increased RANKL production (Elefteriou et al., 2005; Takeda et al., 2002). Thus, our findings from dynamic histomorphometry and skeletal gene expression analyses align with a role for elevated SNS tone in the osteopenia phenotype of 8-month-old male 5xFAD mice. Nevertheless, we could not detect elevated norepinephrine concentrations in plasma or bone in these mice. This finding could reflect problems with sample stability and the poor sensitivity of our methods. Further studies are required to address the potential role of increased SNS activity in the skeletal phenotype of 5xFAD male mice, such as those in which these

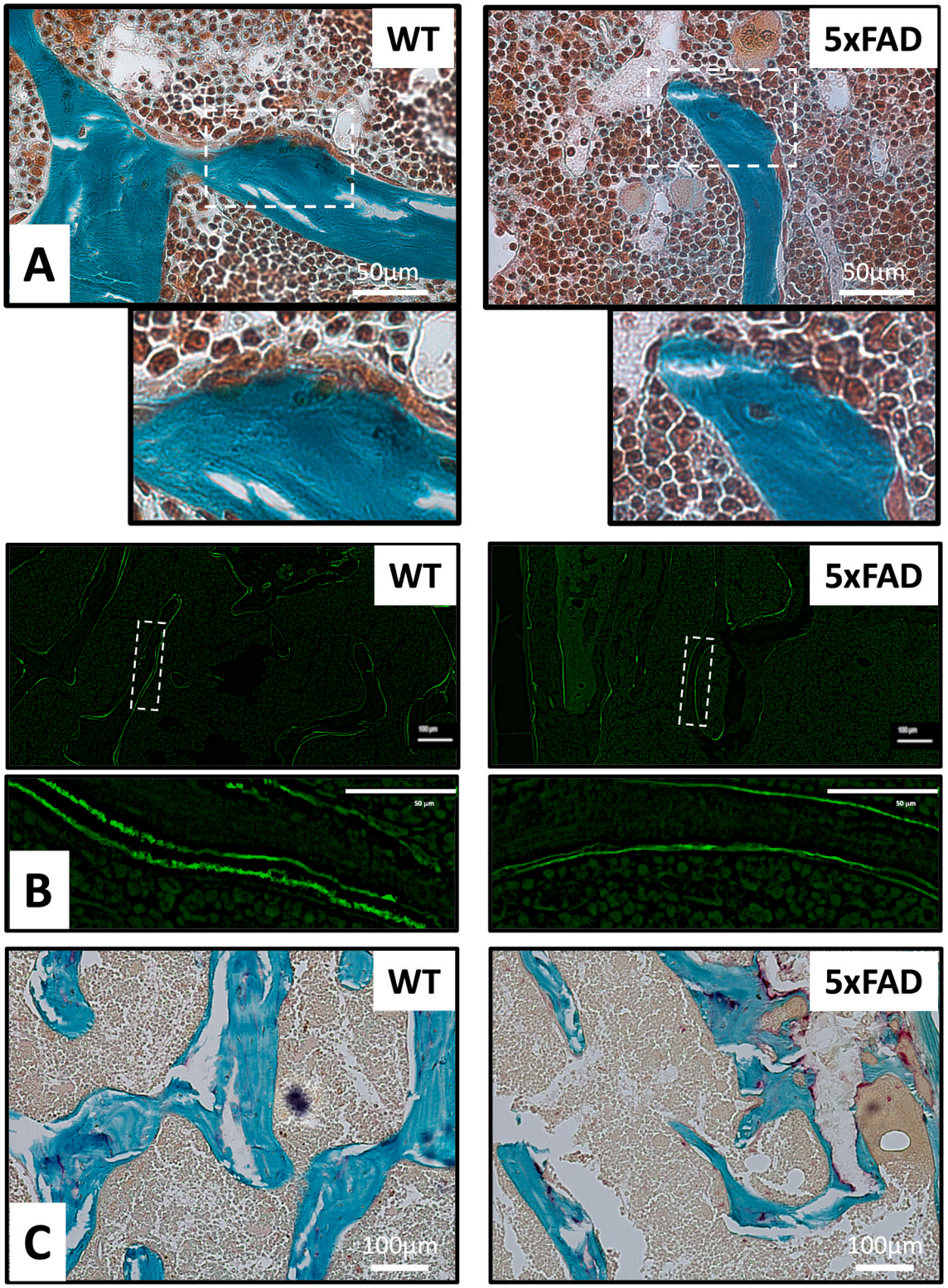

Fig. 3. Histological analysis of femurs from 8-month-old male WT and 5xFAD littermates show reduced bone formation and increased bone resorption parameters. Representative images of bone sections used for histomorphometry: (A) Masson's Trichrome stain used to visualize osteoblasts; (B) Double-calcein labeling used to determine bone formation rate. Two doses of calcein (25 mg/kg) injections with eight days-interval were administered to 8-month-old male WT (n = 9) and 5xFAD mice ($n = 12$) intraperitoneally (*i.p.*); Dotted rectangles in A and B indicate the magnified area presented underneath; (C) TRAP-staining used to identify osteoclasts, with Fast Green as counterstaining.

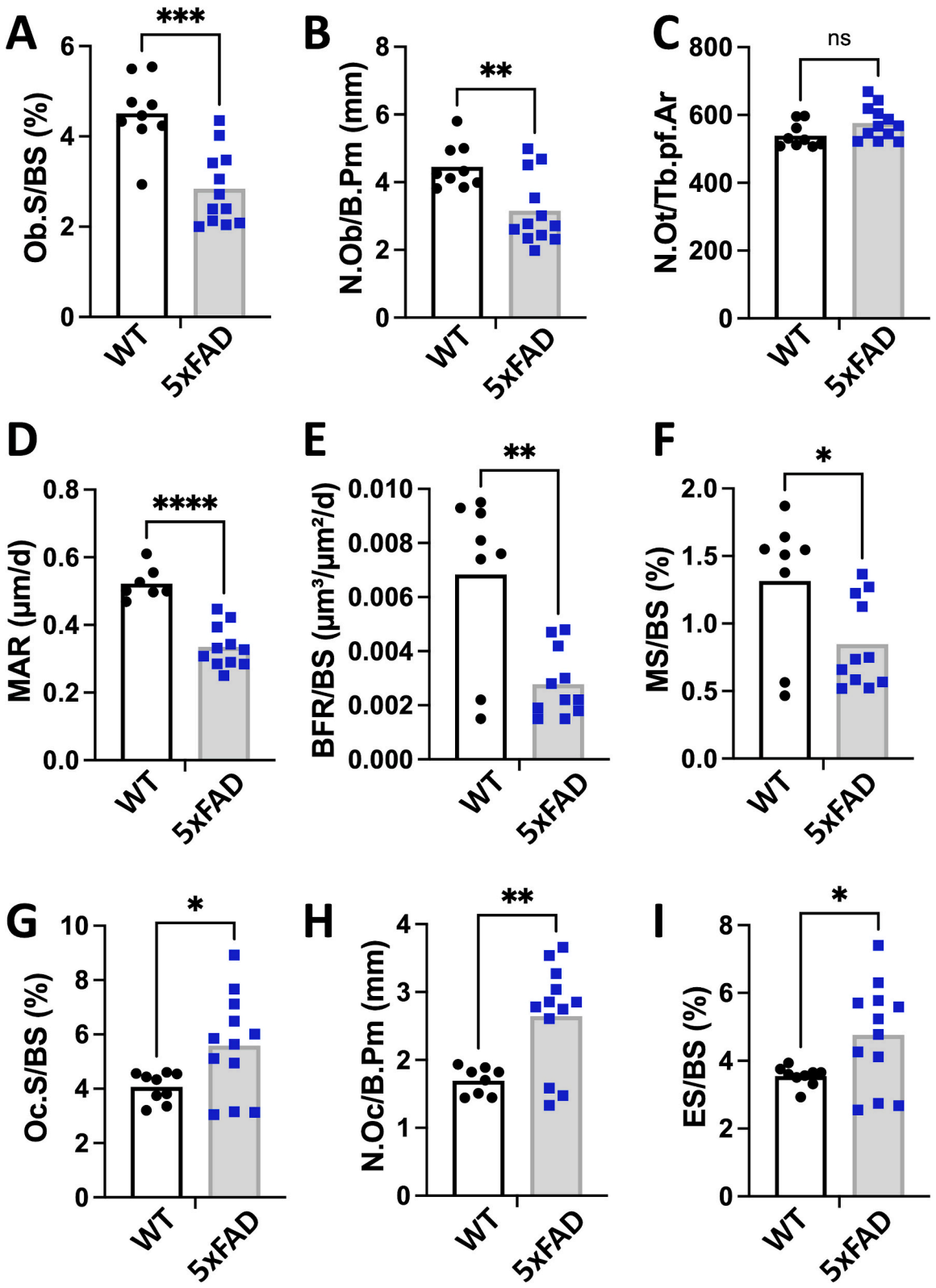

Fig. 4. Histomorphometry reveals decreased bone formation and increased bone resorption in 8-month-old male 5xFAD mice. (A-I) Dynamic histomorphometry analysis showing osteoblast, osteoclast, bone formation, and bone resorption parameters. Two doses of calcein (25 mg/kg) injections with eight days-interval were administered to 8-month-old WT (n = 9) and 5xFAD mice (n = 12) intraperitoneally (*i.p.*). Histomorphometry analyses were performed in the femoral trabecular and cortical bone 72 h after the last calcein injection. Ob.S, osteoblast surface; BS, bone surface; N.Ob, osteoblast number; N.Ot, osteocyte number; Tb.pf.Ar, trabecular bone area; MAR, mineral apposition rate; BFR, bone formation rate; MS, mineralizing surface; Oc.S, osteoclast surface; N.Oc, osteoclast number; B·Pm, bone perimeter; ES, erosion surface. Data represent individual points and mean. *, $P < 0.05$; **, $P < 0.01$; ***, $P < 0.001$; ****, $P < 0.0001$ by Student's t-test; n = 9–12 mice per group.

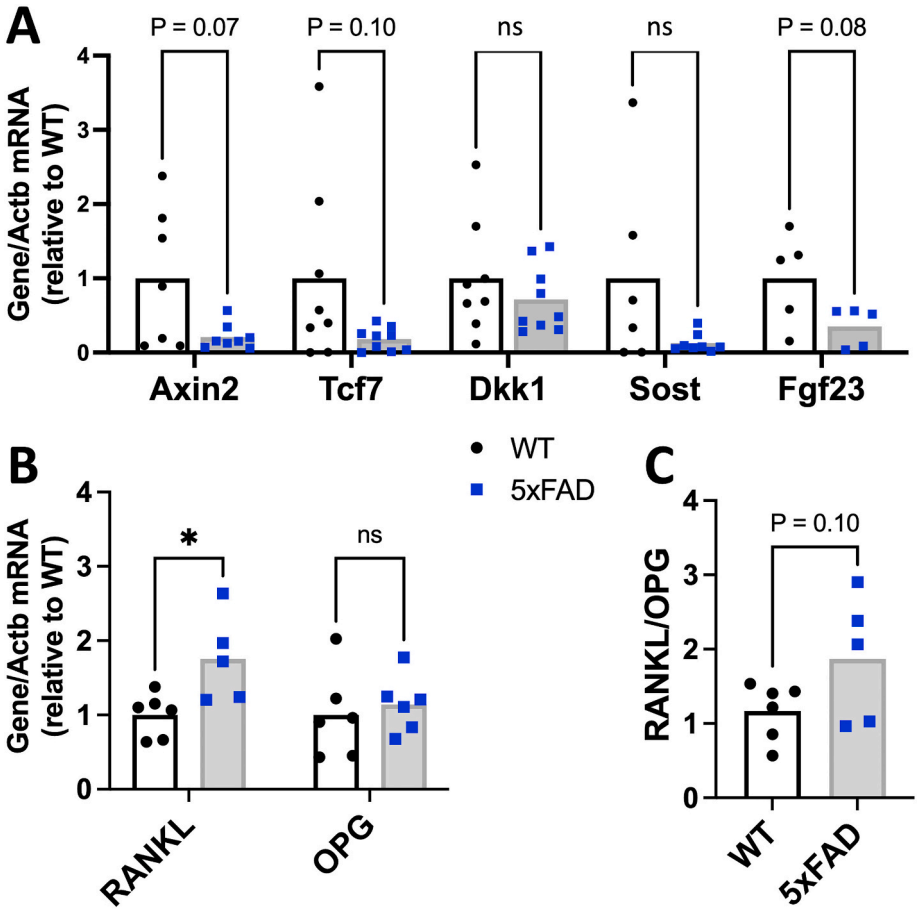

Fig. 5. Eight-month-old male 5xFAD bones show a trend toward diminished levels of Wnt/β-catenin signaling targets and a significant increase in RANKL mRNA. (A) The levels of mRNA encoding Axin-2 (*Axin2*), transcription factor-7 (*Tcf7*), Dickkopf WNT Signaling Pathway Inhibitor 1 (*Dkk1*), and sclerostin (*Sost*), and fibroblast growth factor-23 (*Fgf23*); (B) mRNA levels of *Tnfsf11* (encoding RANKL) and *Tnfrsf11b* (encoding OPG); and (C) the ratio of *Tnfsf11* mRNA to *Tnfrsf11b* mRNA. Total RNA was isolated from the femoral bone after the marrow was flushed out and epiphyses were removed. mRNA levels were quantitated by real-time RT-PCR relative to *β-actin*. Data represent individual points and mean. *, $P < 0.05$ by Student's t-test; ns, not significant; n = 5–9 mice per group.

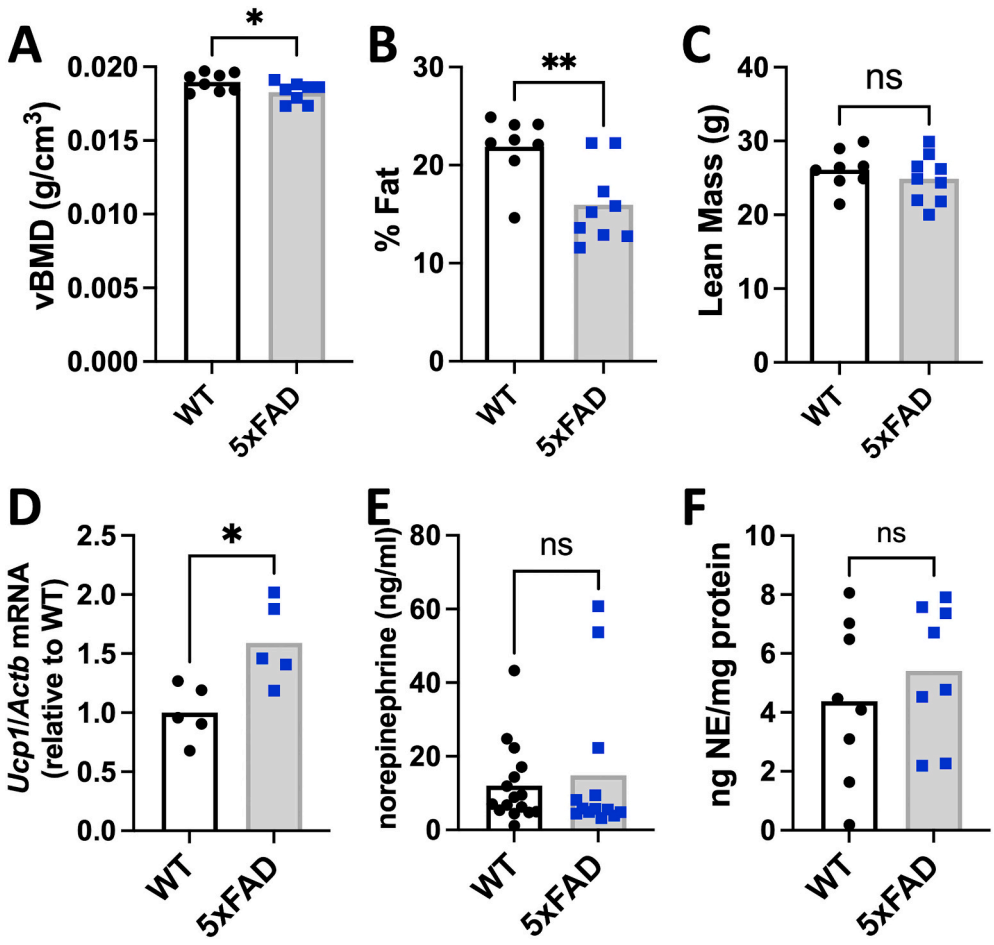

Fig. 6. Male 5xFAD mice exhibit diminished body fat percentage and evidence of increased SNS tone.
(A) Whole body volumetric BMD, (B) percentage of body fat and (C) lean mass of 8-month-old male WT and 5xFAD mice, quantified by DXA analyses (n = 8–9 per group); (D) *Ucp1* mRNA levels in the brown adipose tissue (BAT) of 8-month-old male WT and 5xFAD littermates, measured by real-time RT-PCR relative to β-actin (n = 5 per group); (E) Plasma or (F) cortical bone norepinephrine levels of 8-month-old WT and 5xFAD mice were measured by the High-sensitive ELISA kit; Data represent individual points and mean. *, $p < 0.05$; **, $P < 0.01$ by Student's t-test; ns, not significant; n = 13–16 mice per group.

mice are treated with β-adrenergic receptor blockers.

Consistent with circadian rhythm disturbances in AD patients (Musiek et al., 2015, 2018), aberrant circadian rhythm-related gene expression has also been found in the nervous system of various APP/PS1 mouse models of AD (Jankowsky et al., 2004). Our finding of decreased skeletal *Bmal1* and *Rora* expression levels, with a tendency for altered *Nr1d1*, *Clock,* and *Per1* expression levels may suggest a perturbed circadian rhythm in the bones of male 5xFAD mice. Interestingly, it has been shown that the adrenergic agonist isoproterenol stimulates skeletal *Fgf23* expression and that this stimulation is abrogated in *Bmal1* knockout mice (Kawai et al., 2014). Thus, the diminished levels of skeletal *Fgf23* expression and serum FGF23 in male 5xFAD mice might also partly indicate a disrupted circadian rhythm. Nonetheless, it is important to note that our results were obtained at a single time point rather than multiple time points over a 24-h period, and therefore, we cannot conclude that the skeletal circadian rhythm is indeed altered in this AD mouse model. Aberrant *BMAL1* gene DNA methylation and expression levels have been identified in brain samples and fibroblasts from AD patients (Cronin et al., 2017), suggesting that the neuropathology associated with Aβ may dysregulate this gene's expression in multiple tissues. The lower renal *Bmal1* expression that we found in male 5xFAD mice could reflect a similar phenomenon.

Several studies explored the role of clock genes in skeletal physiology. The ablation of *Bmal1* globally or in osteoblasts enhanced bone resorption due to exuberant osteoclastogenesis associated with elevated RANKL levels (Takarada et al., 2017). Thus, diminished *Bmal1* expression may also contribute to the elevated RANKL expression in male 5xFAD femurs. Another mouse study also demonstrated osteopenia due to BMAL1 deficiency, associated with diminished osteoblasts and osteocytes in vivo and perturbed osteoblastic differentiation of mesenchymal stem cells in vitro (Samsa et al., 2016). These findings suggest that BMAL1 deficiency may contribute to the reduced bone formation parameters observed in 5xFAD males. Contrary to those findings, however, another study revealed an increased bone formation rate and osteoblast numbers in *Bmal1* knockout mice (Fu et al., 2005). In addition, postnatally deleting *Bmal1* in the osteoblast lineage led to progressively augmented trabecular bone mass with modestly reduced cortical bone mass (Qian et al., 2020). Thus, whether the diminished skeletal *Bmal1* expression contributes directly to the skeletal findings in male 5xFAD mice is uncertain. Our analyses were done at a single time point, albeit the same for all mice. Therefore, it is possible that rather than BMAL1 deficiency, the 5xFAD bones had a diurnal BMAL1 rhythm significantly different from that in WT mice.

While we were writing our manuscript, another report described the skeletal phenotype of 5xFAD mice, revealing decreased mineralization, toughness, and quality of cortical bone with endocortical bone loss in both male and female 5xFAD mice at the age of 12 months (LLabre et al., 2022). While sympathetic nervous system activity or circadian clock gene expression was not evaluated, the bone phenotype was found to reflect the accumulation of advanced glycation end products in the bone

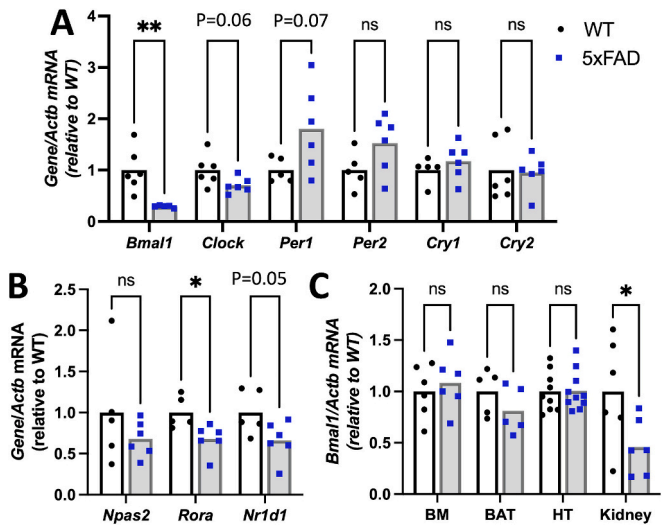

Fig. 7. The expression levels of clock genes are perturbed in bones from 5xFAD males. Expression levels of (A) *Bmal1*, *Clock*, *Per1*, *Per2*, *Cry1*, and *Cry2* and (B) *Npas2*, *Rora*, and *Nr1d1* in femoral bones from 8-month-old male WT and 5xFAD mice. (C) Bone marrow (BM), brown adipose tissue (BAT), hypothalamus (HT), and kidney expression levels of *Bmal1* mRNA in WT and 5xFAD mice. Data represent individual points and mean. *, $p < 0.05$ and **, $p < 0.01$ by Student's t-test; ns, not significant; n = 5–10 mice per group.

matrix. It remains to be determined whether this pathology also contributes to the reduced bone mass we observed in 8-month-old 5xFAD males or develops later to cause bone fragility and loss in a sex-independent manner.

In summary, using an AD mouse model in which Aβ pathology is driven specifically in the brain, we demonstrated that AD-like neuropathology promotes bone loss by decreasing bone formation and increasing bone resorption, likely secondary to elevated SNS tone and perturbed circadian rhythm. The bone loss, however, was observed in male 5xFAD mice only, suggesting that sex-specific factors may play a role in the effect of AD on bone remodeling.

Abbreviations

AD	Alzheimer's disease
5xFAD	five familial Alzheimer's disease
APP	amyloid precursor protein
PSEN1	presenilin 1
WT	wildtype
Aβ	amyloid-β
qRT-PCR	quantitative reverse transcription-polymerase chain reaction
ELISA	enzyme-linked immunosorbent assay
DXA	dual-energy X-ray absorptiometry
μCT	micro-computed tomography
PTH	parathyroid hormone
SNS	sympathetic nervous system
BM	bone marrow
BMSC	bone marrow stromal cells
HT	hypothalamus
BAT	brown adipose tissues
alpha-MEM	alpha-Minimum Essential Medium
i.p.	intraperitoneally
BMD	bone mineral density
BV/TV	bone volume per trabecular volume
Cor Ar/T Ar	cortical area per total area
Ct. TMD	cortical tissue mineral density
Tb. Th	trabecular thickness
Cor. Th	cortical thickness
Ob.S	osteoblast surface
BS	bone surface
N.Ob	osteoblast number
N.Ot	osteocyte number
Tb.pf.Ar	trabecular bone area
MAR	mineral apposition rate
BFR	bone formation rate
MS	mineralizing surface
Oc.S	osteoclast surface
N.Oc	osteoclast number
B·Pm	bone perimeter
ES	erosion surface
ConnD	connectivity
SMI	structure model index
Tb. N	trabecular number
Tb. Sp	trabecular separation
Tt. Ar	total area
Ct. Ar	cortical area
Ct. Porosity	cortical porosity
pMOI	polar moment of inertia
Imax	maximum moment of inertia
Imin	minimum moment of inertia
Wnts	wingless-related integration site
Axin2	AXIS inhibition protein 2
Tcf7	transcription factor-7
Dkk1	dickkopf WNT signaling pathway inhibitor 1
Sost	sclerostin
Fgf23	fibroblast growth factor-23
RANKL	receptor activator of nuclear factor kappa-B ligand
OPG	osteoprotegerin
Tnfsf11	tumor necrosis factor ligand superfamily member 11
Tnfrsf11b	tumor necrosis factor receptor superfamily member 11B
Ucp1	uncoupling protein 1
Bmal1	brain and muscle arnt-like protein-1
Clock	circadian locomotor output cycles kaput
Per1	period circadian regulator 1
Per2	period circadian regulator 2
Cry1	cryptochrome circadian regulator 1
Cry2	cryptochrome circadian regulator 2
NPAS2	neuronal PAS domain protein 2
Rora	RAR-related orphan receptor A
Nr1d1	Nuclear Receptor Subfamily 1 Group D Member 1

CRediT authorship contribution statement

Younghun Jung: Writing – original draft, Methodology, Formal analysis, Data curation, Conceptualization. **Birol Ay:** Writing – original draft, Methodology, Formal analysis, Data curation, Conceptualization. **Sajin M. Cyr:** Methodology, Data curation. **Christina M. Tognoni:** Writing – review & editing, Methodology, Formal analysis, Data curation. **Kaitlin Klovdahl:** Methodology. **Julia Matthias:** Methodology. **Qiuxia Cui:** Methodology. **Daniel J. Brooks:** Methodology, Data curation. **Mary L. Bouxsein:** Writing – review & editing, Resources, Investigation. **Isabel Carreras:** Writing – review & editing, Investigation, Formal analysis, Conceptualization. **Alpaslan Dedeoglu:** Writing – review & editing, Supervision, Resources, Investigation, Funding acquisition, Formal analysis, Conceptualization. **Murat Bastepe:** Writing – review & editing, Writing – original draft, Supervision, Resources, Project administration, Investigation, Funding acquisition, Formal analysis, Data curation, Conceptualization.

Declaration of competing interest

The authors declare that they have no conflict of interest.

Data availability

The data that support the findings of this study are available in the methods and/or supplementary material of this article.

Acknowledgments

This research is supported, in part, by an interim support fund from the MGH Executive Committee on Research (ECOR) and an MGH Center for Skeletal Research Core Small Grant (to MB). It was also supported by NIH/NIDDK and NIH/NIA research grants (R01 DK121776 to MB and RF1 AG056032 to AD). Massachusetts General Hospital, Center for Skeletal Research (CSR), an NIH-funded program (P30 AR075042 from NIAMS) provided the consultation and technical support for skeletal imaging and histology analyses.

Appendix A. Supplementary data

Supplementary data to this article can be found online at https://doi.org/10.1016/j.bonr.2024.101771.

References

Alzheimer's Association, 2014. Alzheimer's & Dementia, 10, e47–e92. https://doi.org/10.1016/j.jalz.2014.02.001.

Arora, D., Robey, P.G., 2022. Recent updates on the biological basis of heterogeneity in bone marrow stromal cells/skeletal stem cells. Biomater Transl 3, 3–16. https://doi.org/10.12336/biomatertransl.2022.01.002.

Ayturk, U.M., Scollan, J.P., Goz Ayturk, D., Suh, E.S., Vesprey, A., Jacobsen, C.M., Divieti Pajevic, P., Warman, M.L., 2020. Single-cell RNA sequencing of calvarial and long-bone endocortical cells. J. Bone Miner. Res. 35, 1981–1991. https://doi.org/10.1002/jbmr.4052.

Baron, R., Gori, F., 2018. Targeting WNT signaling in the treatment of osteoporosis. Curr. Opin. Pharmacol. 40, 134–141. https://doi.org/10.1016/j.coph.2018.04.011.

Baryawno, N., Przybylski, D., Kowalczyk, M.S., Kfoury, Y., Severe, N., Gustafsson, K., Kokkaliaris, K.D., Mercier, F., Tabaka, M., Hofree, M., Dionne, D., Papazian, A., Lee, D., Ashenberg, O., Subramanian, A., Vaishnav, E.D., Rozenblatt-Rosen, O., Regev, A., Scadden, D.T., 2019. A cellular taxonomy of the bone marrow stroma in homeostasis and leukemia. Cell 177, 1915–1932.e16. https://doi.org/10.1016/j.cell.2019.04.040.

Benjamin, R.M., 2010. Bone health: preventing osteoporosis. Public Health Rep. 125, 368–370. https://doi.org/10.1177/003335491012500302.

Black, D.M., Rosen, C.J., 2016. Postmenopausal Osteoporosis. N. Engl. J. Med. 374, 254–262. https://doi.org/10.1056/NEJMcp1513724.

Blennow, K., De Leon, M.J., Zetterberg, H., 2006. Alzheimer's disease. Lancet 368, 387–403. https://doi.org/10.1016/S0140-6736(06)69113-7.

Bliuc, D., Tran, T., Adachi, J.D., Atkins, G.J., Berger, C., Van Den Bergh, J., Cappai, R., Eisman, J.A., Van Geel, T., Geusens, P., Goltzman, D., Hanley, D.A., Josse, R., Kaiser, S., Kovacs, C.S., Langsetmo, L., Prior, J.C., Nguyen, T.V., Solomon, L.B., Stapledon, C., Center, J.R., For the Canadian Multicentre Osteoporosis Study (CaMos) Research Group, 2021. Cognitive decline is associated with an accelerated rate of bone loss and increased fracture risk in women: a prospective study from the Canadian Multicentre Osteoporosis Study. J. Bone Miner. Res. 36, 2106–2115. https://doi.org/10.1002/jbmr.4402.

Bolsius, Y.G., Zurbriggen, M.D., Kim, J.K., Kas, M.J., Meerlo, P., Aton, S.J., Havekes, R., 2021. The role of clock genes in sleep, stress and memory. Biochem. Pharmacol. 191, 114493 https://doi.org/10.1016/j.bcp.2021.114493.

Bouxsein, M.L., Boyd, S.K., Christiansen, B.A., Guldberg, R.E., Jepsen, K.J., Müller, R., 2010. Guidelines for assessment of bone microstructure in rodents using micro-computed tomography. J. Bone Miner. Res. 25, 1468–1486. https://doi.org/10.1002/jbmr.141.

Canet, G., Chevallier, N., Zussy, C., Desrumaux, C., Givalois, L., 2018. Central role of glucocorticoid receptors in Alzheimer's disease and depression. Front. Neurosci. 12, 739. https://doi.org/10.3389/fnins.2018.00739.

Carter, D.R., Bouxsein, M.L., Marcus, R., 1992. New approaches for interpreting projected bone densitometry data. J. Bone Miner. Res. 7, 137–145. https://doi.org/10.1002/jbmr.5650070204.

Chen, X.D., Qian, H.Y., Neff, L., Satomura, K., Horowitz, M.C., 1999. Thy-1 antigen expression by cells in the osteoblast lineage. J. Bone Miner. Res. 14, 362–375. https://doi.org/10.1359/jbmr.1999.14.3.362.

Chen, Y.-H., Lo, R., 2017. Alzheimer's disease and osteoporosis. Tzu Chi Med J 29, 138. https://doi.org/10.4103/tcmj.tcmj_54_17.

Compston, J.E., McClung, M.R., Leslie, W.D., 2019. Osteoporosis. Lancet 393, 364–376. https://doi.org/10.1016/S0140-6736(18)32112-3.

Craig, S.E.L., Michalski, M.N., Williams, B.O., 2023. Got WNTS? Insight into bone health from a WNT perspective. Curr. Top. Dev. Biol. 153, 327–346. https://doi.org/10.1016/bs.ctdb.2023.01.004.

Cronin, P., McCarthy, M.J., Lim, A.S.P., Salmon, D.P., Galasko, D., Masliah, E., De Jager, P.L., Bennett, D.A., Desplats, P., 2017. Circadian alterations during early stages of Alzheimer's disease are associated with aberrant cycles of DNA methylation in BMAL1. Alzheimers Dement. 13, 689–700. https://doi.org/10.1016/j.jalz.2016.10.003.

Cui, Q., Aksu, C., Ay, B., Remillard, C.E., Plagge, A., Gardezi, M., Dunlap, M., Gerstenfeld, L.C., He, Q., Bastepe, M., 2021. Maternal GNAS contributes to the extra-large G protein α-subunit (XLαs) expression in a cell type-specific manner. Front. Genet. 12, 680537 https://doi.org/10.3389/fgene.2021.680537.

Cui, S., Xiong, F., Hong, Y., Jung, J.-U., Li, X.-S., Liu, J.-Z., Yan, R., Mei, L., Feng, X., Xiong, W.-C., 2011. APPswe/Aβ regulation of osteoclast activation and RAGE expression in an age-dependent manner. J. Bone Miner. Res. 26, 1084–1098. https://doi.org/10.1002/jbmr.299.

Cummings, S.R., Melton, L.J., 2002. Epidemiology and outcomes of osteoporotic fractures. Lancet 359, 1761–1767. https://doi.org/10.1016/S0140-6736(02)08657-9.

Dempster, D.W., Compston, J.E., Drezner, M.K., Glorieux, F.H., Kanis, J.A., Malluche, H., Meunier, P.J., Ott, S.M., Recker, R.R., Parfitt, A.M., 2013. Standardized nomenclature, symbols, and units for bone histomorphometry: a 2012 update of the report of the ASBMR Histomorphometry nomenclature committee. J. Bone Miner. Res. 28, 2–17. https://doi.org/10.1002/jbmr.1805.

Dengler-Crish, C.M., Smith, M.A., Wilson, G.N., 2016. Early evidence of low bone density and decreased serotonergic synthesis in the dorsal raphe of a tauopathy model of Alzheimer's disease. JAD 55, 1605–1619. https://doi.org/10.3233/JAD-160658.

Dengler-Crish, C.M., Ball, H.C., Lin, L., Novak, K.M., Cooper, L.N., 2018. Evidence of Wnt/β-catenin alterations in brain and bone of a tauopathy mouse model of Alzheimer's disease. Neurobiol. Aging 67, 148–158. https://doi.org/10.1016/j.neurobiolaging.2018.03.021.

Dimitri, P., Rosen, C., 2017. The central nervous system and bone metabolism: an evolving story. Calcif. Tissue Int. 100, 476–485. https://doi.org/10.1007/s00223-016-0179-6.

Driessler, F., Baldock, P.A., 2010. Hypothalamic regulation of bone. J. Mol. Endocrinol. 45, 175–181. https://doi.org/10.1677/JME-10-0015.

Elefteriou, F., Ahn, J.D., Takeda, S., Starbuck, M., Yang, X., Liu, X., Kondo, H., Richards, W.G., Bannon, T.W., Noda, M., Clement, K., Vaisse, C., Karsenty, G., 2005. Leptin regulation of bone resorption by the sympathetic nervous system and CART. Nature 434, 514–520. https://doi.org/10.1038/nature03398.

Elrod, R., Peskind, E.R., DiGiacomo, L., Brodkin, K.I., Veith, R.C., Raskind, M.A., 1997. Effects of Alzheimer's disease severity on cerebrospinal fluid norepinephrine concentration. Am. J. Psychiatry 154, 25–30. https://doi.org/10.1176/ajp.154.1.25.

Esang, M., Gupta, M., 2021. Aducanumab as a novel treatment for Alzheimer's disease: a decade of hope, controversies, and the future. Cureus. https://doi.org/10.7759/cureus.17591.

Fu, L., Patel, M.S., Bradley, A., Wagner, E.F., Karsenty, G., 2005. The molecular clock mediates leptin-regulated bone formation. Cell 122, 803–815. https://doi.org/10.1016/j.cell.2005.06.028.

Glatt, V., Canalis, E., Stadmeyer, L., Bouxsein, M.L., 2007. Age-related changes in trabecular architecture differ in female and male C57BL/6J mice. J. Bone Miner. Res. 22, 1197–1207. https://doi.org/10.1359/jbmr.070507.

Harvey, N., Dennison, E., Cooper, C., 2010. Osteoporosis: impact on health and economics. Nat. Rev. Rheumatol. 6, 99–105. https://doi.org/10.1038/nrrheum.2009.260.

Idelevich, A., Baron, R., 2018. Brain to bone: what is the contribution of the brain to skeletal homeostasis? Bone 115, 31–42. https://doi.org/10.1016/j.bone.2018.05.018.

Ishii, M., Iadecola, C., 2015. Metabolic and non-cognitive manifestations of Alzheimer's disease: the hypothalamus as both culprit and target of pathology. Cell Metab. 22, 761–776. https://doi.org/10.1016/j.cmet.2015.08.016.

Iwaniec, U.T., Turner, R.T., 2016. Influence of body weight on bone mass, architecture and turnover. J. Endocrinol. 230, R115–R130. https://doi.org/10.1530/JOE-16-0089.

Jankowsky, J.L., Fadale, D.J., Anderson, J., Xu, G.M., Gonzales, V., Jenkins, N.A., Copeland, N.G., Lee, M.K., Younkin, L.H., Wagner, S.L., Younkin, S.G., Borchelt, D. R., 2004. Mutant presenilins specifically elevate the levels of the 42 residue beta-amyloid peptide in vivo: evidence for augmentation of a 42-specific gamma secretase. Hum. Mol. Genet. 13, 159–170. https://doi.org/10.1093/hmg/ddh019.

Karner, C.M., Long, F., 2017. Wnt signaling and cellular metabolism in osteoblasts. Cell. Mol. Life Sci. 74, 1649–1657. https://doi.org/10.1007/s00018-016-2425-5.

Kawai, M., Kinoshita, S., Shimba, S., Ozono, K., Michigami, T., 2014. Sympathetic activation induces skeletal Fgf23 expression in a circadian rhythm-dependent manner. J. Biol. Chem. 289, 1457–1466. https://doi.org/10.1074/jbc.M113.500850.

Khandelwal, S., Lane, N.E., 2023. Osteoporosis: review of etiology, mechanisms, and approach to management in the aging population. Endocrinol. Metab. Clin. N. Am. 52, 259–275. https://doi.org/10.1016/j.ecl.2022.10.009.

Kostev, K., Hadji, P., Jacob, L., 2018. Impact of osteoporosis on the risk of dementia in almost 60,000 patients followed in general practices in Germany. JAD 65, 401–407. https://doi.org/10.3233/JAD-180569.

Larkin, H.D., 2023. Lecanemab gains FDA approval for early Alzheimer disease. JAMA 329, 363. https://doi.org/10.1001/jama.2022.24490.

Lavi-Moshayoff, V., Wasserman, G., Meir, T., Silver, J., Naveh-Many, T., 2010. PTH increases FGF23 gene expression and mediates the high-FGF23 levels of experimental kidney failure: a bone parathyroid feedback loop. American Journal of Physiology-Renal Physiology 299, F882–F889. https://doi.org/10.1152/ajprenal.00360.2010.

Liu, S., Tang, W., Fang, J., Ren, J., Li, H., Xiao, Z., Quarles, L.D., 2009. Novel regulators of Fgf23 expression and mineralization in Hyp bone. Mol. Endocrinol. 23, 1505–1518. https://doi.org/10.1210/me.2009-0085.

LLabre, J.E., Gil, C., Amatya, N., Lagalwar, S., Possidente, B., Vashishth, D., 2022. Degradation of bone quality in a transgenic mouse model of Alzheimer's disease. J. Bone Miner. Res. 37, 2548–2565. https://doi.org/10.1002/jbmr.4723.

Loskutova, N., Honea, R.A., Brooks, W.M., Burns, J.M., 2010. Reduced limbic and hypothalamic volumes correlate with bone density in early Alzheimer's disease. JAD 20, 313–322. https://doi.org/10.3233/JAD-2010-1364.

Lv, X.-L., Zhang, J., Gao, W.-Y., Xing, W.-M., Yang, Z.-X., Yue, Y.-X., Wang, Y.-Z., Wang, G.-F., 2018. Association between osteoporosis, bone mineral density levels and Alzheimer's disease: a systematic review and Meta-analysis. Int. J. Gerontol. 12, 76–83. https://doi.org/10.1016/j.ijge.2018.03.007.

Marazuela, P., Paez-Montserrat, B., Bonaterra-Pastra, A., Solé, M., Hernández-Guillamon, M., 2022. Impact of cerebral amyloid angiopathy in two transgenic mouse models of cerebral β-amyloidosis: a neuropathological study. IJMS 23, 4972. https://doi.org/10.3390/ijms23094972.

Moechars, D., Lorent, K., De Strooper, B., Dewachter, I., Van Leuven, F., 1996. Expression in brain of amyloid precursor protein mutated in the alpha-secretase site causes disturbed behavior, neuronal degeneration and premature death in transgenic mice. EMBO J. 15, 1265–1274. https://doi.org/10.1002/j.1460-2075.1996.tb00468.x.

Musiek, E.S., Xiong, D.D., Holtzman, D.M., 2015. Sleep, circadian rhythms, and the pathogenesis of Alzheimer disease. Exp. Mol. Med. 47, e148 https://doi.org/10.1038/emm.2014.121.

Musiek, E.S., Bhimasani, M., Zangrilli, M.A., Morris, J.C., Holtzman, D.M., Ju, Y.-E.S., 2018. Circadian rest-activity pattern changes in aging and preclinical Alzheimer disease. JAMA Neurol. 75, 582–590. https://doi.org/10.1001/jamaneurol.2017.4719.

Nagata, Y., Imanishi, Y., Tateishi, T., Miyaoka, D., Kurajoh, M., Arnold, A., Emoto, M., 2022. Parathyroid hormone regulates circulating levels of sclerostin and FGF23 in a primary hyperparathyroidism model. Journal of the Endocrine Society 6, bvac027. https://doi.org/10.1210/jendso/bvac027.

Oakley, H., Cole, S.L., Logan, S., Maus, E., Shao, P., Craft, J., Guillozet-Bongaarts, A., Ohno, M., Disterhoft, J., Van Eldik, L., Berry, R., Vassar, R., 2006. Intraneuronal beta-amyloid aggregates, neurodegeneration, and neuron loss in transgenic mice with five familial Alzheimer's disease mutations: potential factors in amyloid plaque formation. J. Neurosci. 26, 10129–10140. https://doi.org/10.1523/JNEUROSCI.1202-06.2006.

Okamura, H., 2007. Suprachiasmatic nucleus clock time in the mammalian circadian system. Cold Spring Harb. Symp. Quant. Biol. 72, 551–556. https://doi.org/10.1101/sqb.2007.72.033.

Pascualy, M., Petrie, E.C., Brodkin, K., Peskind, E.R., Wilkinson, C.W., Raskind, M.A., 2000. Hypothalamic pituitary adrenocortical and sympathetic nervous system responses to the cold pressor test in Alzheimer's disease. Biol. Psychiatry 48, 247–254. https://doi.org/10.1016/S0006-3223(00)00879-9.

Peng, W., Li, Z., Guan, Y., Wang, D., Huang, S., 2016. A study of cognitive functions in female elderly patients with osteoporosis: a multi-center cross-sectional study. Aging Ment. Health 20, 647–654. https://doi.org/10.1080/13607863.2015.1033680.

Peng, Y., Liu, Jing, Tang, Y., Liu, Jianshu, Han, T., Han, S., Li, H., Hou, C., Liu, Jiankang, Long, J., 2014. High-fat-diet-induced weight gain ameliorates bone loss without exacerbating $A\beta^2$PP processing and cognition in female APP/PS1 mice. Front. Cell. Neurosci. 8 https://doi.org/10.3389/fncel.2014.00225.

Percie du Sert, N., Ahluwalia, A., Alam, S., Avey, M.T., Baker, M., Browne, W.J., Clark, A., Cuthill, I.C., Dirnagl, U., Emerson, M., Garner, P., Holgate, S.T., Howells, D.W., Hurst, V., Karp, N.A., Lazic, S.E., Lidster, K., MacCallum, C.J., Macleod, M., Pearl, E.J., Petersen, O.H., Rawle, F., Reynolds, P., Rooney, K., Sena, E. S., Silberberg, S.D., Steckler, T., Würbel, H., 2020. Reporting animal research: explanation and elaboration for the ARRIVE guidelines 2.0. PLoS Biol. 18, e3000411 https://doi.org/10.1371/journal.pbio.3000411.

Qian, Z., Zhang, Ying, Kang, X., Li, H., Zhang, Yan, Jin, X., Gao, X., Xu, M., Ma, Z., Zhao, L., Zhang, Z., Sun, H., Wu, S., 2020. Postnatal conditional deletion of Bmal1 in osteoblasts enhances trabecular bone formation via increased BMP2 signals. J. Bone Miner. Res. 35, 1481–1493. https://doi.org/10.1002/jbmr.4017.

Raskind, M.A., Peskind, E.R., Veith, R.C., Beard, J.C., Gumbrecht, G., Halter, J.B., 1988. Increased plasma and cerebrospinal fluid norepinephrine in older men: differential suppression by clonidine*. J. Clin. Endocrinol. Metab. 66, 438–443. https://doi.org/10.1210/jcem-66-2-438.

Samsa, W.E., Vasanji, A., Midura, R.J., Kondratov, R.V., 2016. Deficiency of circadian clock protein BMAL1 in mice results in a low bone mass phenotype. Bone 84, 194–203. https://doi.org/10.1016/j.bone.2016.01.006.

Saper, C.B., German, D.C., 1987. Hypothalamic pathology in Alzheimer's disease. Neurosci. Lett. 74, 364–370. https://doi.org/10.1016/0304-3940(87)90325-9.

Sivaraj, K.K., Jeong, H.-W., Dharmalingam, B., Zeuschner, D., Adams, S., Potente, M., Adams, R.H., 2021. Regional specialization and fate specification of bone stromal cells in skeletal development. Cell Rep. 36, 109352 https://doi.org/10.1016/j.celrep.2021.109352.

Szot, P., Leverenz, J.B., Peskind, E.R., Kiyasu, E., Rohde, K., Miller, M.A., Raskind, M.A., 2000. Tyrosine hydroxylase and norepinephrine transporter mRNA expression in the locus coeruleus in Alzheimer's disease. Mol. Brain Res. 84, 135–140. https://doi.org/10.1016/S0169-328X(00)00168-6.

Takarada, T., Xu, C., Ochi, H., Nakazato, R., Yamada, D., Nakamura, S., Kodama, A., Shimba, S., Mieda, M., Fukasawa, K., Ozaki, K., Iezaki, T., Fujikawa, K., Yoneda, Y., Numano, R., Hida, A., Tei, H., Takeda, S., Hinoi, E., 2017. Bone resorption is regulated by circadian clock in osteoblasts. J. Bone Miner. Res. 32, 872–881. https://doi.org/10.1002/jbmr.3053.

Takeda, S., Elefteriou, F., Levasseur, R., Liu, X., Zhao, L., Parker, K.L., Armstrong, D., Ducy, P., Karsenty, G., 2002. Leptin regulates bone formation via the sympathetic nervous system. Cell 111, 305–317. https://doi.org/10.1016/S0092-8674(02)01049-8.

Thomas, S.A., Palmiter, R.D., 1997. Thermoregulatory and metabolic phenotypes of mice lacking noradrenaline and adrenaline. Nature 387, 94–97. https://doi.org/10.1038/387094a0.

Tysiewicz-Dudek, M., Pietraszkiewicz, F., Drozdzowska, B., 2008. Alzheimer's disease and osteoporosis: common risk factors or one condition predisposing to the other? Ortop. Traumatol. Rehabil. 10, 315–323.

Vercruysse, P., Vieau, D., Blum, D., Petersén, Å., Dupuis, L., 2018. Hypothalamic alterations in neurodegenerative diseases and their relation to abnormal energy metabolism. Front. Mol. Neurosci. 11, 2. https://doi.org/10.3389/fnmol.2018.00002.

Vidal, M., Morris, R., Grosveld, F., Spanopoulou, E., 1990. Tissue-specific control elements of the Thy-1 gene. EMBO J. 9, 833–840. https://doi.org/10.1002/j.1460-2075.1990.tb08180.x.

Xia, W.-F., Jung, J.-U., Shun, C., Xiong, S., Xiong, L., Shi, X.-M., Mei, L., Xiong, W.-C., 2013. Swedish mutant APP suppresses osteoblast differentiation and causes osteoporotic deficit, which are ameliorated by N-acetyl-L-cysteine: APP INHIBITS BONE FORMATION. J. Bone Miner. Res. 28, 2122–2135. https://doi.org/10.1002/jbmr.1954.

Xing, L., Schwarz, E.M., Boyce, B.F., 2005. Osteoclast precursors, RANKL/RANK, and immunology. Immunol. Rev. 208, 19–29. https://doi.org/10.1111/j.0105-2896.2005.00336.x.

Yang, M.-W., Wang, T.-H., Yan, P.-P., Chu, L.-W., Yu, J., Gao, Z.-D., Li, Y.-Z., Guo, B.-L., 2011. Curcumin improves bone microarchitecture and enhances mineral density in APP/PS1 transgenic mice. Phytomedicine 18, 205–213. https://doi.org/10.1016/j.phymed.2010.05.011.

Yoshioka, H., Okita, S., Nakano, M., Minamizaki, T., Nubukiyo, A., Sotomaru, Y., Bonnelye, E., Kozai, K., Tanimoto, K., Aubin, J.E., Yoshiko, Y., 2021. Single-cell RNA-sequencing reveals the breadth of osteoblast heterogeneity. JBMR Plus 5, e10496. https://doi.org/10.1002/jbm4.10496.

Youlten, S.E., Kemp, J.P., Logan, J.G., Ghirardello, E.J., Sergio, C.M., Dack, M.R.G., Guilfoyle, S.E., Leitch, V.D., Butterfield, N.C., Komla-Ebri, D., Chai, R.C., Corr, A.P., Smith, J.T., Mohanty, S.T., Morris, J.A., McDonald, M.M., Quinn, J.M.W., McGlade, A.R., Bartonicek, N., Jansson, M., Hatzikotoulas, K., Irving, M.D., Beleza-Meireles, A., Rivadeneira, F., Duncan, E., Richards, J.B., Adams, D.J., Lelliott, C.J., Brink, R., Phan, T.G., Eisman, J.A., Evans, D.M., Zeggini, E., Baldock, P.A., Bassett, J. H.D., Williams, G.R., Croucher, P.I., 2021. Osteocyte transcriptome mapping identifies a molecular landscape controlling skeletal homeostasis and susceptibility to skeletal disease. Nat. Commun. 12, 2444. https://doi.org/10.1038/s41467-021-22517-1.

Zhu, Y., Ma, Y., Elefteriou, F., 2018. Cortical bone is an extraneuronal site of norepinephrine uptake in adult mice. Bone Reports 9, 188–198. https://doi.org/10.1016/j.bonr.2018.11.002.